Polar correlations and defect-induced ferroelectricity in cryogenic $KTaO_3$

Oktay Aktas,[1,*] Sam Crossley,[2] Michael A. Carpenter,[1] and Ekhard K. H. Salje[1]

[1]*University of Cambridge, Department of Earth Sciences, Downing Street, Cambridge CB2 3EQ, United Kingdom*

[2]*University of Cambridge, Department of Materials Science, Pembroke Street, Cambridge CB2 3QZ, United Kingdom*

(Received 22 July 2014; revised manuscript received 4 September 2014; published 27 October 2014)

$KTaO_3$ is an incipient ferroelectric material with an extrapolated transition temperature below 0 K. It contains a small number of "unavoidable defects" which are randomly distributed. Some of these defects are polar and their interaction leads to macroscopic coherent polar structures at low temperatures. In this article it is shown that freezing of local defect dipoles coincides with elastic stiffening and damping of ultrasonic waves in $KTaO_3$. The elastic freezing anomalies are accompanied by stepwise increases of piezoelectricity, forming a thermal polar staircase below ca. 120 K and a gigantic enhancement below 50 K. A small spontaneous polarization also emerges below this temperature, gradually increasing to a value of 0.045 μC cm^{-2} at 5 K with increasing coherency of defect dipoles. The orientation of this spontaneous polarization depends on a weak strain-induced anisotropy of the macroscopic sample. Defect-induced ferroelectricity, as demonstrated for $KTaO_3$, may be a possible way forward to develop functional device materials based on the switching of coherently interacting defects.

DOI: 10.1103/PhysRevB.90.165309 PACS number(s): 75.10.−b, 75.30.Kz, 75.40.Cx, 62.20.de

I. INTRODUCTION

$KTaO_3$ is an incipient ferroelectric with defect-induced polarity and magnetism on a local scale [1–8]. Defects are abundant even in nominally pure $KTaO_3$, including magnetic elements Fe and Mn and oxygen vacancies [9–12]. In addition, ferroelectricity becomes stable when $KTaO_3$ is doped with Li or Nb [1,3,13,14] and ferroelectricity and ferromagnetism are expected to coexist in suitably doped samples [15]. It is less obvious, however, whether local dipolar configurations can generate macroscopic polarity and piezoelectricity at low doping levels, which requires that the local ferroic properties become coherent over the entire sample. In this paper we show experimentally that such coherency does indeed exist at cryogenic temperatures even when only "unavoidable" impurities exist in the sample. In addition, coherency among these defect dipoles leads to a small spontaneous polarization below 20 K. Eliseev *et al.* [8] have already argued that magnetism occurs for extremely low doping levels near sample surfaces and becomes measurable in nanocrystals [15]. This implies that $KTaO_3$ may be magnetoelectric even for small doping levels and hence a useful material for electronic storage devices [16,17]. $KTaO_3$ is also an ideal relaxorlike material [18] which never becomes ferroelectric. Local dipoles create polar nanoregions (PNR's) which are highly dispersed. The key question is then whether a coherency temperature T^* exists where PNR's switch coherently under electric fields [19].

The coherence length, r_c, for polar correlations increases with increasing dielectric susceptibility which is linked with the incipient ferroelectricity of $KTaO_3$ [20,21]. The extrapolated ferroelectric transition temperature is between 0 K and −10 K [Fig. 1(a); also Refs. [22,23]]. $KTaO_3$ is close to a ferroelectric quantum critical point at zero temperature and has extremely large dielectric constants [24]. Quantum fluctuations destroy the ferroelectric ground state [25–27] while the matrix is strongly polarizable, with local defects generating local dipolar states. This situation is similar to the incipient ferroelectrics $SrTiO_3$ and $CaTiO_3$, where the equivalent "defects" are ferroelastic twin boundaries which are known to contain layers of polar material even when the bulk is nonpolar [28–33]. The interaction between twin boundaries is weak and it is still an open question whether field-induced coherency between polar twin boundaries exists, e.g., via local vortex fields. $KTaO_3$ is not ferroelastic and therefore does not contain twin boundaries which could lead to polar behavior. We may then ask the following: is the propensity of polar point defects to generate local polar structures in a nonpolar matrix sufficient to generate macroscopic polarity if the diluted point defects interact due to lattice deformations, i.e., via strain fields, or via dielectric fields? This question is crucial for the analysis of experimental data in the field of multiferroics and could also be expressed in terms of whether multiferroicity is always a bulk phenomenon or whether it can arise by interaction of some small number of defects to generate weak but finite ferroelectricity macroscopically. It also relates to the issue of whether the quantum critical points in $KTaO_3$ and $SrTiO_3$ are intrinsic or defect mediated [24].

Defects in $KTaO_3$ were studied in single crystals [13,20,34–36] with concentrations lower than the threshold for the defect plateau effect where defects become coherent via direct lattice interactions [20,27]. Details of various point defects were reported before [10–12,37] and the term "unavoidable" defects was introduced to draw attention to the fact that even the most pure samples still have defect concentrations of some 10^{17} cm^{-3} [10], leading to a maximum in the dielectric loss tangent that follows the Arrhenius relationship (see Fig. 1 and its caption). Virtually all defects, such as Li, Mn, Fe, Ta^{4+}, and oxygen vacancies, are known to break the local inversion symmetry [2,10,12,38,39]. In this paper, we show, first, that in a nominally pure single crystal these defect dipoles are not randomly oriented at low temperatures, second, that coherency effects become strong when the temperatures decrease below 120 K, and, third, that these increase dramatically below 50 K. $KTaO_3$ may then be ferroelectric with a small spontaneous polarization (0.04 μC/cm^2) below 20 K.

*oa252@cam.ac.uk

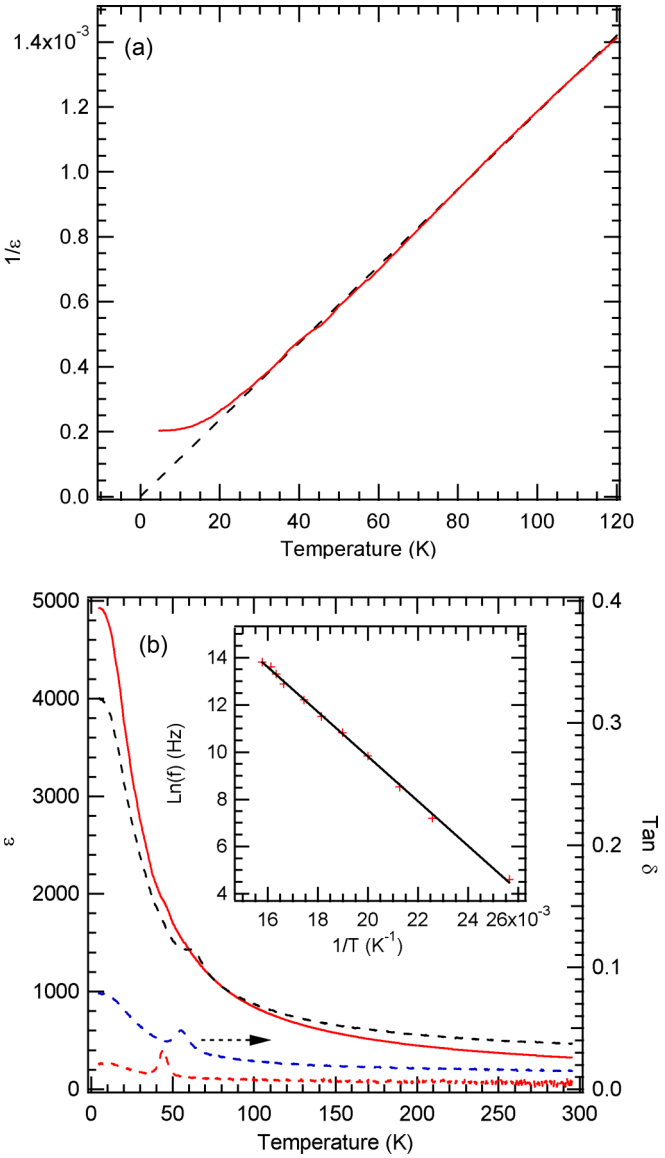

FIG. 1. (Color online) Dielectric constant of single crystal $KTaO_3$ as a function of temperature. (a) The inverse dielectric constant measured at 1.3 kHz extrapolates to a temperature below 0 K, indicating the incipient ferroelectric nature of $KTaO_3$. (b) Dielectric constant measured at 1.3 kHz (continuous line) and $\tan\delta$ measured at 1.3 kHz, 100 kHz, and 820 kHz (represented by red, blue, and black dashed lines, respectively), between 5 K and 300 K. The inset is an Arrhenius plot where f is the measuring frequency and T the temperature at which $\tan\delta$ shows a maximum. This shows a good fit to $\tau = \tau_0 \exp(E_a/k_B T)$, where τ is the relaxation time, k_B is the Boltzmann constant, the activation energy, E_a, is 81 meV, and $1/\tau_0 = 2.2 \times 10^{12}$ s^{-1}.

II. EXPERIMENT

To detect polar correlations in $KTaO_3$ we used resonant piezoelectric spectroscopy (RPS) [40,41] and resonant ultrasound spectroscopy (RUS) [42] between 8 K and 300 K. The *a priori* condition to detect an RPS signal is the existence of macroscopic dipoles which can couple with an external electric field. Randomly oriented dipoles do not produce RPS signals, such as in glass, and there has to be at last some coherence between the polar regions [41,43,44]. RUS involves purely mechanical relaxations. All measurements were performed on a sample of single crystal $KTaO_3$ purchased from MTI Corporation, USA. It was oriented along the cubic axes with dimensions $5 \times 5 \times 0.5$ mm^3 and had a mass of 0.0928 g. The sample was checked for magnetic impurities using a vibrating sample magnetometer; none were found within a resolution of 1 ppm. Although the sample remains cubic macroscopically and is supposed to be optically isotropic, weak optical birefringence was observed in a polarizing microscope, as shown in Fig. 2. White areas reflecting birefringence are almost uniformly distributed with some bigger areas in between. This is attributed to symmetry breaking due to the influence of extrinsic and intrinsic point defects, such as Li, and oxygen vacancies [2,10,12,38,39].

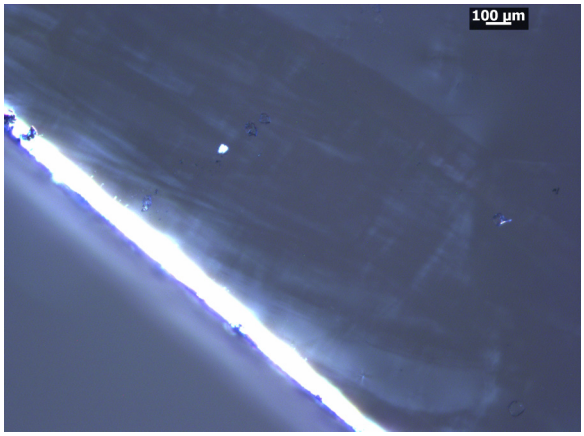

FIG. 2. (Color online) Image of the $KTaO_3$ single crystal sample taken with a polarizing microscope, indicating the existence of weak birefringence due to defects. The white region is one of the edges of the sample. The scale bar is shown on the top right corner of the figure.

For RPS measurements an ac voltage of 25 V was applied across the largest parallel surfaces which were covered with a thin layer of silver paste as electrodes. Using an Orange 50-mm helium flow cryostat [45], individual RPS spectra were collected with 130 000 data points between 100 kHz and 1200 kHz at temperatures between 8 and 300 K in a heating sequence. Without removing the sample from the setup, RUS spectra were collected in the same frequency and temperature range in a separate heating sequence. A 20 min settle time was allowed for thermal equilibration at each temperature before data collection. Then, the sample was removed from the cryostat and remounted to repeat the RPS measurements. Finally, the electrodes were removed and the RUS measurements repeated (8–300 K, 130 000 data points between 80 and 1200 kHz) to make sure that they were not influenced by the coating of silver paste. RUS spectra of the sample without electrodes were also collected between 300 K and 650 K in a heating sequence, using a horizontal resistance furnace in which the sample was supported between the tips of alumina buffer rods [46]. Each spectrum had 50 000 data points in the frequency range 120–1200 kHz. RPS and RUS data were analyzed using the software package IGOR PRO (Wavemetrics). The peak frequency, f, full width at

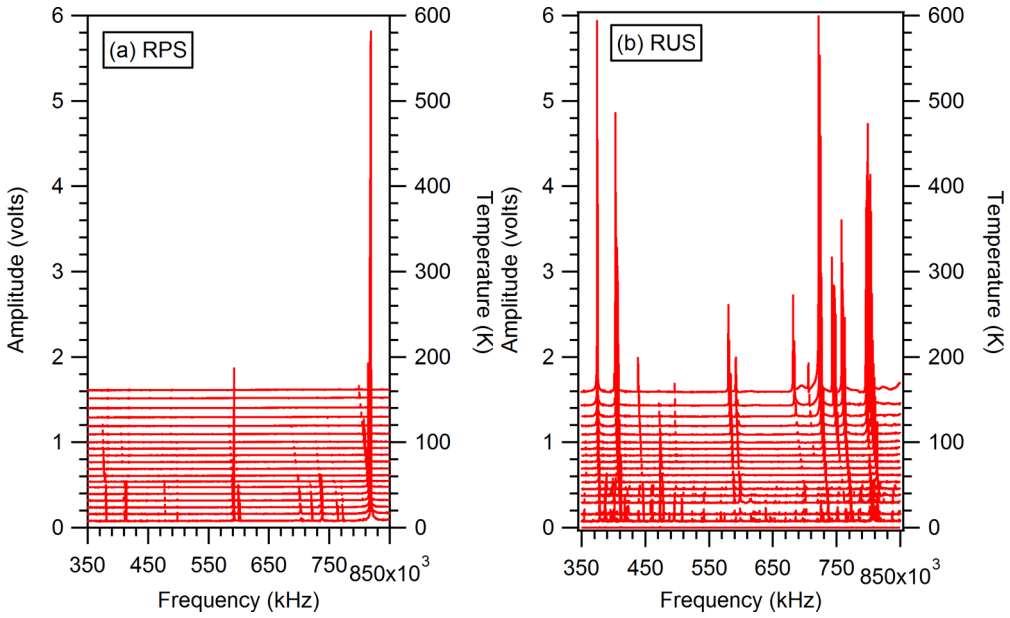

FIG. 3. (Color online) Segments of (a) RPS and (b) RUS spectra collected between 7 K and 160 K in a heating sequence. For these measurements 25 V was applied across the sample or the emitter transducer, for RPS and RUS, respectively. In both panels, the left vertical axis corresponds to amplitude and the right vertical axis is temperature. The spectra have been translated up the y axis in proportion to the temperature at which they were collected and the right vertical axis has been labeled accordingly.

half maximum, Δf, amplitude, and area associated with each mechanical resonance mode were determined by fitting with an asymmetric Lorentzian function. f^2 scales with the magnitude of the elastic constant(s) which determines the resonance, and the inverse mechanical quality factor, Q^{-1}, is given by $\Delta f/f$. Peak areas were determined by integration of the asymmetric Lorentzian curve fit to each peak and subtracting a baseline.

For dielectric constant and polarization measurements, the largest surfaces of the sample were plated with Au to form electrodes with area 10.5 mm^2. The sample was mounted in vacuum on a copper heat reservoir in a probe that was inserted into liquid helium. Impedance spectra were collected using an Agilent 4294A analyzer between 1.3 kHz and 1 MHz. The capacitance of the sample was estimated using a parallel equivalent circuit model. Hysteresis loops of polarization versus electric field [$P(E)$] were measured between 5 K and 160 K at 1 Hz with driving voltages of 440 V ($\sim$8 kV/cm) using a Radiant Precision Premier II tester and external amplifier (Trek 609E-6).

III. RESULTS AND DISCUSSION

Figure 3 shows stacks of RPS and RUS spectra collected between 10 K and 160 K. These data correspond to the first set of RPS and RUS measurements, performed consecutively in separate heating sequences without disturbing the sample in the cryostat. Individual RPS and RUS spectra display increasing frequency with decreasing temperature. In the RUS spectra, some peaks appear below $\sim$50 K and soften down to 10 K. These peaks are not sample peaks and might be resonances associated with the instrument. Values of f for other resonance peaks in RUS spectra and those obtained using RPS are essentially the same, whether the resonance modes are excited electrically (RPS) or mechanically (RUS; see Fig. 10 in the Appendix). The most remarkable feature, however, is that RPS peak intensities increase dramatically with decreasing temperature, while RUS peaks decrease in intensity. Since RPS peaks are generated through the (inverse) macroscopic piezoelectric effect, they give a measure of effective piezoelectric coupling strength [41]. Here, any possible flexoelectricity that may arise from the top transducer resting on the sample is negligible as the weight of the block with the top transducer is very small. We rule out any strong influence from a possible experimental artifact that may be thought to give rise to the additional peaks observed in the RUS spectra [Fig. 3(b)]. As will be seen in the remainder of the paper, these additional peaks were not observed in the RPS measurements and the second RUS run (with no electrodes). The decrease in the RUS peak amplitudes was also observed in the second RUS run, in contrast with the temperature evolution of RPS peaks whose amplitudes drastically increase with decreasing temperature.

The RPS peak area in Fig. 4(a) of the resonance near $f = 820$ kHz shows a 120-fold increase of the RPS amplitude between 150 K and 20 K. This gigantic enhancement proves an increased piezoelectric coupling. The increase has a smooth background superimposed by steps. When the RPS measurements were repeated (with the sample remounted), these results were qualitatively reproduced. In Fig. 3 the first increase in d occurs at 120 K, indicated by a black arrow (I). Upon further cooling a more gradual increase appears at $\sim$60 K (II), followed by sharp increases at $\sim$50 K, $\sim$30 K, and $\sim$20 K (III, IV, and V). Note that the intensity of this resonance is much larger than other peaks in the RPS spectra and enabled us to observe these stepwise increases in d. With other peaks, anomalies at IV and V could not be resolved due to scatter of data points below 50 K. In contrast to the results from RPS and as also seen in Fig. 4(a), the RUS peak area

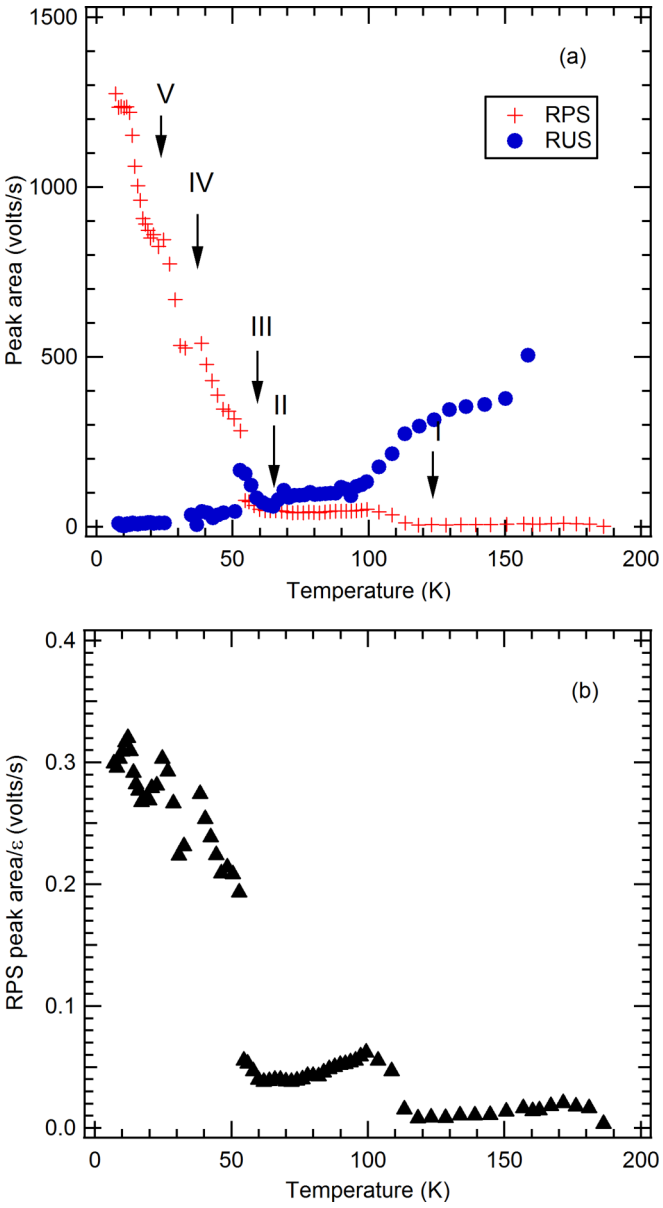

FIG. 4. (Color online) (a) Peak area of the resonance mode at $f \sim 820$ kHz as a function of temperature obtained from RPS (red plus signs) and RUS (blue circles) spectra displayed in Fig. 3. Numbers with black arrows show where the peak area displays stepwise changes at certain temperatures, indicating an enhanced piezoelectric coupling with falling temperature. Panel (b) shows a plot of peak area/dielectric constant against temperature, which represents the qualitative temperature evolution of the piezoelectric charge coefficient $g = d/\epsilon$.

decreases with lowering temperature. At 20 K, the peak area is 50 times smaller than that observed at 158 K.

The inverse piezoelectric coupling coefficient, d, could be thought to be directly correlated with the increase of the dielectric coefficient ϵ at low temperatures ($d = g\epsilon$) where g is the piezoelectric charge coefficient excluding the enhancing effect of the polarizable matrix. This is not the case, however. Figure 4(b) shows as measure for g the ratio between the RPS intensity divided by the dielectric constant. The ratio $g = d/\epsilon$ still increases strongly with decreasing temperature.

Considering the highly polarizable nature of the $KTaO_3$ lattice, we also obtained $P(E)$ loops densely spaced in 5–50 K (a selection of these loops are shown in Fig. 5). The linear dielectric response dominates over any ferroelectric switching effects. There is partial saturation at 5 K, but by 50 K the response is purely linear. We evaluated the pyroelectric coefficient $dP/dT(T)$ by numerically transposing, smoothing (using a cubic spline fit), and differentiating the $P(E)$ loops. Pyroelectric data thus obtained (corresponding to a bias field of 8 kV cm^{-1}) are given in Fig. 6, revealing minima at ~20 K and ~ 45 K which correspond within error to features IV and V from the RPS data [Fig. 4(a)].

To further investigate the presence of ferroelectric switching, we obtained $P(E)$ data using a double wave driving profile to evaluate major and minor $P(E)$ loops. By subtracting minor from major loops to yield remnant or "PUND" (positive up negative down) loops we eliminate time-independent losses and linear dielectric contributions, leaving only ferroelectric switching (if any), time-dependent parasitics (likely small), and noise. This process is described in, e.g., Fukunaga [47] and the exact version of the method we used is described in Ref. [48]. Within these assumptions, the range of P-axis data in the PUND loops is an approximation to twice the nominal spontaneous polarization P_S. According to our data for nominal $P_S(T)$, Fig. 7(a), the trend is a gradual increase upon cooling from 50 K to reach ~ 0.045 μC/cm^2 at 5 K. The PUND loops at 5 K [Fig. 7(b)] and 36.5 K [Fig. 7(d)] show negative curvature of the lower branch, which may be taken as evidence of a ferroelectric switching. This negative curvature is not apparent at the local maxima of 20 K [Fig. 7(c)], suggesting that the applied field of ~8 kV cm^{-1} was subcoercive at those temperatures.

Spontaneous polarization presented in Fig. 7(a) corresponds to switchable polarization. Peaks located at 20 and 35 K, which correspond within error to features IV and V, can be attributed to the freezing out of some defect dipoles. Initially these defect dipoles switch and coherently oscillate with the bias field. With decreasing temperature, some defect dipoles freeze-out and do not respond to the bias field, leading to a peak in the polarization in their temperature evolution. Similar peaks could be expected in the derivative of the dielectric constant with respect to temperature. But we could not resolve these peaks with our data. Stepwise increases of the RPS signal in Fig. 4 as well as those in the pyroelectric coefficient (Fig. 6), and the possible remanent polarization observed below 50 K (Figs. 5 and 7), are related to the freezing of different local defects [2,10–12,39]. This freezing could also appear in the RUS spectra in the form of peaks in mechanical damping, together with steplike changes in elastic constants typical of Debye-like freezing processes [49–51]. Peaks in damping measured as a function of temperature can be used to calculate the activation energy E_a associated with each freezing process using [52]

$$Q^{-1} = Q_m^{-1}\left\{\cosh\frac{E_a}{Rr_2}\left(\frac{1}{T}-\frac{1}{T_m}\right)\right\}^{-1}, \qquad (1)$$

where Q_m^{-1} is the maximum value of the inverse mechanical quality factor, R is the gas constant, and r_2 is the spectral width. Figure 8 depicts mechanical damping, expressed as Q^{-1} for

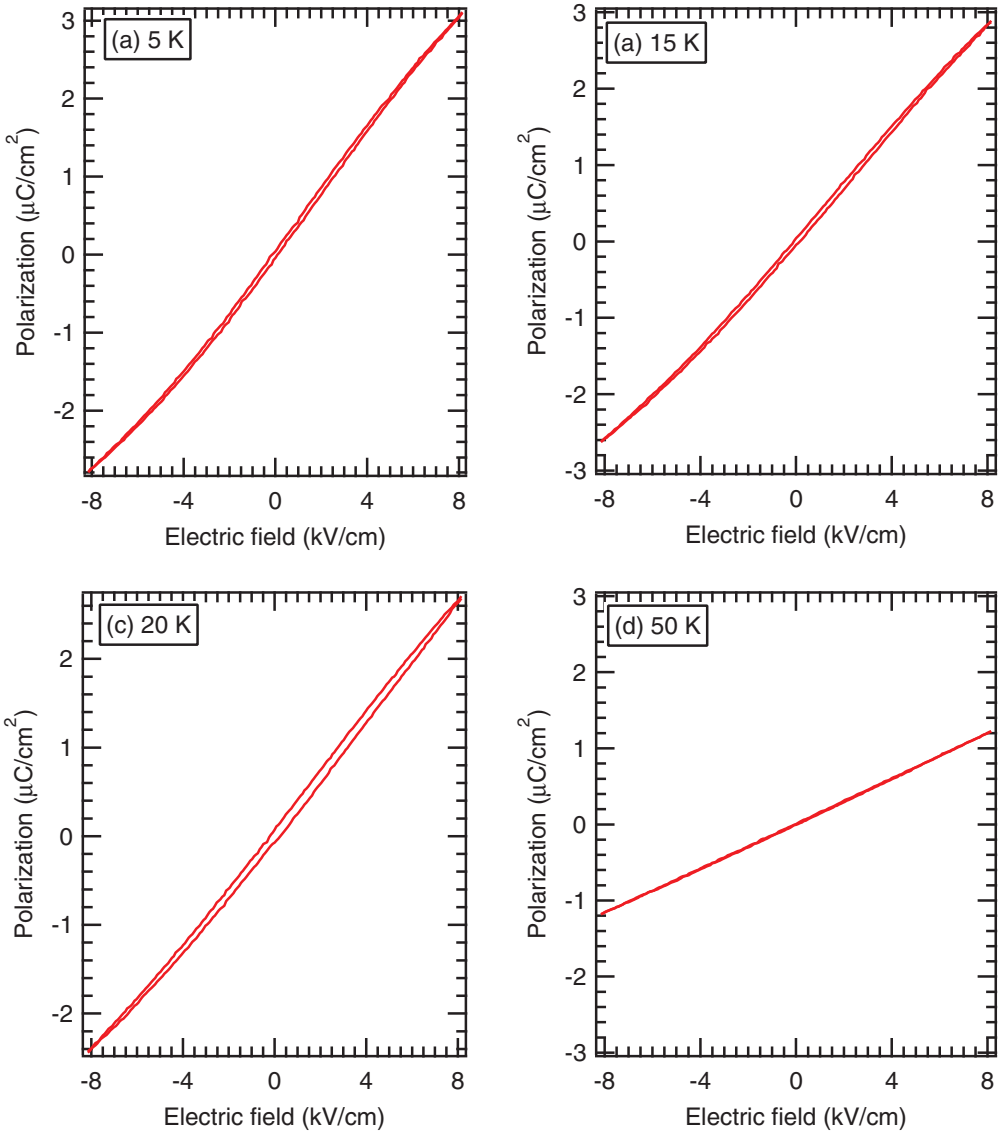

FIG. 5. (Color online) Polarization-electric field loops of single crystal $KTaO_3$ obtained at 1 Hz using a 540 μm thick sample: (a) 5 K; (b) 15 K; (c) 20 K; (d) 50 K.

resonance peaks with frequencies in the range 80–1180 kHz. To rule out any possible influence of sample electrodes on the frequency and mechanical damping, we present the results from RUS measurements performed after the removal of the sample electrodes (see Fig. 11 in the Appendix).

Three distinct peaks occur in the mechanical damping at low temperatures. A fit using Eq. (1) with $r_2 = 1$ leads to 86 meV for peak II [Fig. 8(b)]. This activation energy corresponds to the reorientation motion of Li^+ impurities (<0.01%) on the K^+ site according to Laguta *et al.* [37]. The small Li ions rattle in the large 12-fold coordinated oxygen site and generate local dipoles. It is possible that the Li dipoles polarize adjacent lattice units, leading to small polar nanoregions. The Q^{-1} peak for $f = 500$ kHz at 50 K gives $E_a = 70$ meV, which is in agreement with the activation energy (70–90 meV) determined from dielectric loss spectra [11,20,37]. Laguta *et al.* [37] argued that this peak is due to impurities of Li while Fe^{3+} were also proposed [12]. Charge neutrality is expected through oxygen vacancies V_O, creating a dipolar defect pair, e.g., Fe^{3+}-V_O. Regardless of its origin, this defect leads to a peak in the dielectric loss tangent even in ultrapure samples [12], as also seen in our dielectric measurements presented in Fig. 1(b) ($E_a = 86$ meV). Finally, a fit to the peak in Q^{-1} for $f \approx 85$ kHz located at ≈ 30 K (IV) leads to $E_a = 31$ meV ($r_2 = 1$). According to electron spin resonance measurements performed after UV light illumination [10], there are three Ta^{4+} centers that create dipolar defect pairs with oxygen vacancies: Ta^{4+}-V_O, Ta^{4+}-OH^-, and Ta^{4+}-V_O-Me^{4+}, where Me^{4+} is a dopant ion. The first two centers are stable up to a temperature between 30 K and 35 K. The activation energy for Ta^{4+}-V_O was reported as 26 meV [10], which is close to the value determined using the data for mechanical damping. The third Ta^{4+} center, Ta^{4+}-V_O-Me^{4+}, is reported by Laguta *et al.* [10] to have an activation energy of 8 meV. These are stable up to ≈ 15 K, which perhaps explains the stepwise increase in piezoelectric coupling observed around 20 K (V in Fig. 4). Mechanical

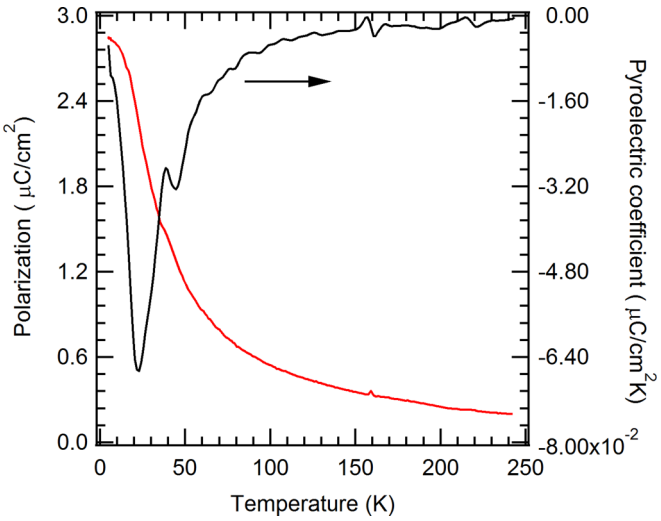

FIG. 6. (Color online) Polarization and pyroelectric coefficient (dP/dT) of $KTaO_3$ obtained by the application of 440 V across a 540 μm thick sample in a heating sequence.

damping shown in Fig. 8 does not show an equivalent peak around 20 K within experimental resolution. The increase in the peak area (V) could also originate from Ta^{4+}-V_O and Ta^{4+}-OH^- dipoles as the intensities of the corresponding ESR lines make a dip at 20 K and then increase at lower temperatures. Considering that Ta^{4+} ions were not observed in nonilluminated crystals [10], the increase in RPS peak area at ≈30 K (IV) and ≈20 K (V) might correspond to dipolar defects of different origins.

Resonances with $f \sim 150$ kHz, 370 kHz, and 880 kHz have broad peaks in Q^{-1} located between 100 K and 150 K, which roughly coincide with the temperature (120 K) at which piezoelectric coupling increases (I). The nature of the increase near 120 K is not known as no such anomaly has been reported before when the defect chemistry was analyzed [10–12]. A possible correlation can be made with Fe^{3+}-O_I dipoles, where O_I is an interstitial oxygen, which lead to peaks at 150 and 175 K at 1 kHz, although an increase in the peak area in Fig. 6 (or inverse piezoelectric coupling) would be expected above 200 K as the frequency of this resonance (820 kHz) is much higher [37].

Taking into account increased mechanical damping around room temperature (Fig. 8), RUS measurements were performed between 300 K and 650 K after the removal of the electrodes (see Fig. 12). These measurements, along with those performed at low temperatures (Fig. 11), revealed another peak in mechanical damping near 320 K for a resonance at $f \sim 500$ kHz) with an activation energy of 0.51 eV [Fig. 8(c)]. This might perhaps be associated with oxygen vacancies whose activation energies for diffusion range from 0.1 eV to 0.9 eV in perovskites [22,53].

As each peak of the mechanical damping must be accompanied by an increase in resonance frequencies, which is proportional to the effective elastic modulus, we present in Fig. 9(a) the temperature evolution of the squared frequency of a resonance mode with f near 150 kHz. These results were obtained from the same RUS spectra (Fig. 11) that were used to determine mechanical damping (Fig. 8). The squared frequency shows a change of slope in the linear temperature dependence (red line) near 170 K. It is interesting to note that a similar deviation from a linear temperature dependence can also be seen in the dielectric constant in the same temperature range, as shown in the lower inset of Fig. 9(a). On the other hand, the squared frequency of another resonance mode with $f \approx 500$ kHz [Fig. 9(b)] remains linear down to 60 K. The different behavior of the two modes suggests that they are governed by different effective elastic moduli. Using the mode at 500 kHz, the quantum saturation temperature θ_s for elastic moduli can be calculated using $f^2 = m + n\theta_s \coth \theta_s/T$, where m and n are constants [55], and the fit shown in Fig. 9(b) gives $\theta_s = 40$ K. This value is different for the thermal expansion with $\theta_s = 196$ K, determined from the variation of the lattice constant measured by Abe *et al.* [54] [inset in Fig. 9(a)]. The different values for θ_s indicate that the moduli do not harden simply because the molar volume decreases, but that interatomic changes also contribute to the elastic hardening [56].

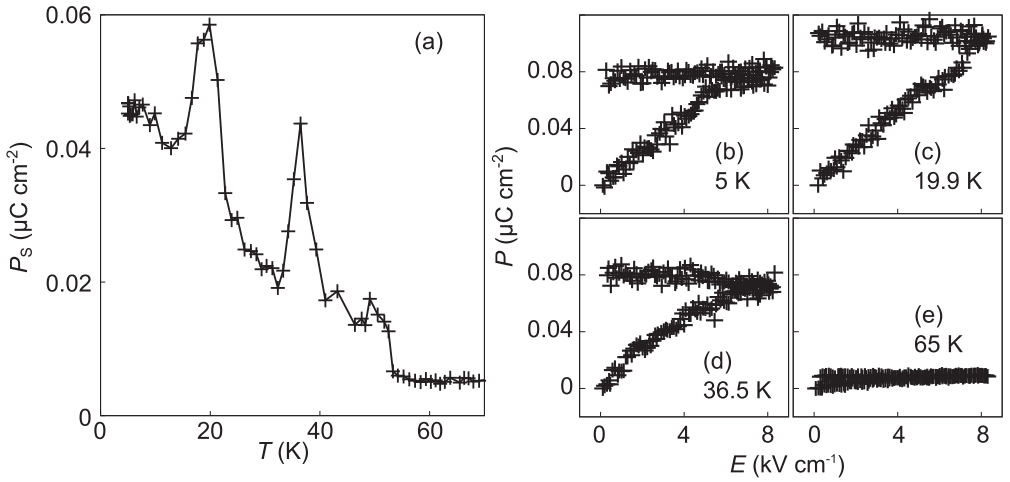

FIG. 7. (a) Nominal spontaneous polarization evaluated using "PUND" $P(E)$ loops. (b)–(e) Specimen PUND loops from the data set used to compile (a).

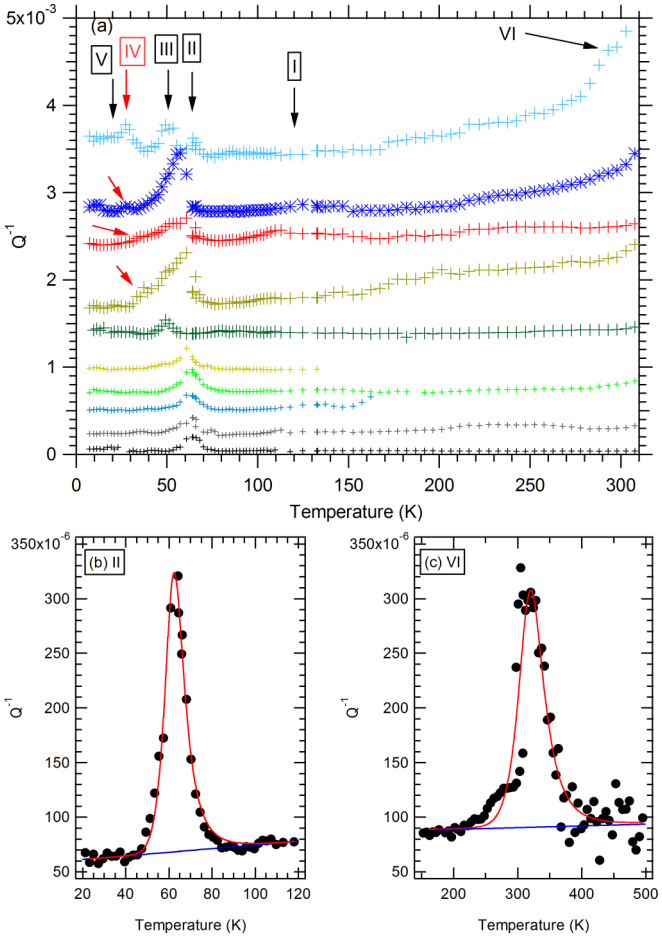

FIG. 8. (Color online) Mechanical damping, expressed in terms of Q^{-1}, associated with individual peaks from the RUS spectra of $KTaO_3$. (a) Temperature evolution of Q^{-1} between 8 K and 300 K obtained using the RUS spectra presented in Fig. 11 (see Appendix). From the upper curve to the lowest, mode frequencies at 10 K are approximately 84 kHz, 150 kHz, 370 kHz, 425 kHz, 500 kHz, 592 kHz, 740 kHz, 880 kHz, 1140 kHz, and 1180 kHz. See caption of Fig. 4 and text for the description of numbers I, II, III, IV, V, and VI. (b) A peak in Q^{-1} located at ~60 K (II) for the mode at 740 kHz and the fit using Eq. (1) (red line), for which the baseline (blue line) was also taken into account gives $E_a = 86$ meV. (c) A peak at 320 K (VI) in Q^{-1} for the mode located at 500 kHz obtained using the spectra presented in Figs. 11 and 12. The fit using Eq. (1), the red line, yields $E_a = 0.51$ eV.

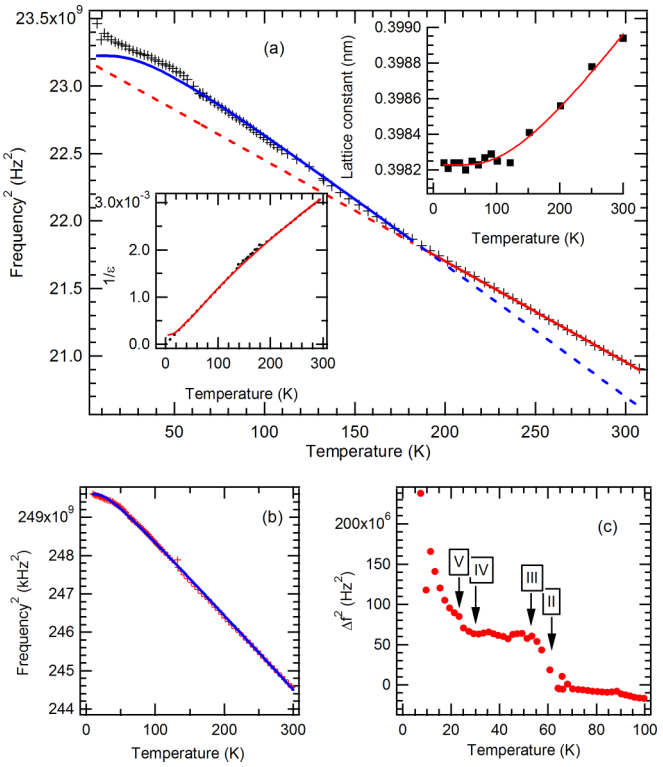

FIG. 9. (Color online) Temperature evolution of the squared frequency of a resonance mode ($f \sim 150$ kHz) between 10 K and 300 K. Plus signs correspond to the data, which deviate from the linear regime near 170 K, as indicated by the red line. The lower inset shows that a deviation from the linear temperature dependence, indicated by dotted black lines, has also been observed in the dielectric constant in the same temperature range. The blue line is the baseline $f^2 = m + n\theta_s \coth \theta_s / T$, where m and n are constants and $\theta_s = 40$ K is the quantum saturation temperature. Upper inset in panel (a) shows the temperature evolution of the lattice constant extracted from Abe *et al.* [54] and a fit using $a = m + n\theta_s \coth \theta_s / T$ with $\theta_s = 196$ K. For the baseline $\theta_s = 40$ K was determined using the resonance mode at 500 K shown in (b). (c) A plot of $\Delta f^2 = f^2 - f^2_{\text{baseline}}$ for the mode presented in panel (a). Numbers II, III, IV, and V correspond to those presented in Fig. 4 and are used to indicate anomalies in the frequency.

Small stepwise increases (II, IV, and V) of the squared frequency are also visible below ~65 K in Fig. 9(a). These are seen more clearly in the temperature evolution of $\Delta f^2 = f^2 - f^2_{\text{baseline}}$, where f^2_{baseline} denotes the blue baseline in Fig. 9(a) which has been fit with $\theta_s = 40$ K. They coincide with the temperatures of the loss peaks (Fig. 8) and with temperatures where the RPS peak areas increase by steps (Fig. 4). Hence the freezing of local dipoles does indeed increase the elastic stiffness of $KTaO_3$. By analogy with incipient ferroelectrics, one may question whether $KTaO_3$ is also an incipient proper ferroelastic [57], in which case softening of elastic moduli would be expected at low temperatures. Elastic hardening shown in Fig. 9 rules out the possibility that the incipient transition is driven by a proper elastic instability, and improper ferroelasticity is likely if the sample becomes tetragonal [58]. Even in that case, elastic precursor effects are extremely weak in $KTaO_3$, in contrast with materials like $PbSc_{0.5}Ta_{0.5}O_3$, which also contains significant structural disorder [41].

Data represented in Figs. 9(a) and 9(c) are obtained from a resonance peak whose frequency (150 kHz) is different than that of the resonance used to obtain Fig. 4 (820 kHz). We chose to use the peak at 150 kHz (for the analysis presented in Fig. 9) because this peak has a very smooth temperature evolution, which made it possible to extract very small frequency anomalies (II, IV, and V) presented in Fig. 9(c). The absence of an anomaly associated with III in the Δf^2 data could be attributed to the fact that a certain defect dipole may oscillate at a particular frequency but not necessarily other. It might also be that the jump indicated by II might actually stem

from both II and III and we cannot resolve the two expected jumps as the temperatures at which they would be observed are close.

Our results have implications for the understanding of the coherency temperature T^* in highly diluted relaxors [18,19]. The onset of the coherency [19] of polar nanoregions (PNR's) at some temperature T^* can be contrasted with relaxors where coherent dipoles stem from strain modulations of the crystal structure at temperatures above the structural transition point T_c. In this case the relaxor structure is related to tweed [40,41,44] and not the appearance of PNR's as ferroelectric precursors. In $KTaO_3$ the strain effect is very weak because the incipient transition is polar but not ferroelastic, and tweed nanostructures are hence expected to remain very weak. Highly diluted defect structures are present, however, so that the development of their coherency contains the same physical mechanism as the increase of coherency near T^* in defect induced relaxors. From our data, T^* is then estimated to be near 60 K.

Samara and Morosin [59] determined the saturation temperature from their dielectric data using the Barrett equation and found $T_1 = 60$ K, close to the (main) onset of collective excitations T^* (Fig. 4). The agreement between T_1 and T^* is, of course, expected. The temperature T_1 reflects the value of the fluctuation variance [55] whereby the highest saturation temperature dominates whenever several variances overlap [60]. It was shown that the empirical value of T_1 can usually be related to the highest frequency excitation [60]. Thus it appears that the anomaly at T^* determines the value of T_1. The determination of T_1 is only approximate in the paper of Samara and Morosin [59] and it will not be possible to determine the exact link of the dispersion correction or the possible coupling between different excitations.

The symmetry conditions for piezoelectricity are the same as for optical second harmonic generation, SHG, for which strong signature have been observed in $KTaO_3$ [61]. The difference is that SHG probes local structural deviations [62], while our results show that (part of) the local structural distortion becomes coherent and hence macroscopic. The physical picture is that point defects in $KTaO_3$ form dipoles, which are (mostly) randomly oriented at high temperatures. With decreasing temperature, the dipole field increases because the dielectric susceptibility increases but also because direct lattice interactions increase and thermal randomization decreases. At the freezing points of the multiple defects we find that the reduced orientational mobility leads to increased structural stiffness accompanied by peaks in mechanical damping. As our results show a direct correlation between freezing of defect dipoles and increased macroscopic dipole moment, the piezoelectricity cannot be just related to flexoelectric effects near surfaces [63]. The simultaneous increase of the piezocoefficient, g, shows that the freezing of switchable defect dipoles is not random but favors parallel arrangements of the dipoles and hence macroscopic polarity. This polarity increases greatly at very low temperatures and leads to weak ferroelectricity below 50 K. This result agrees well with the observations of Goloviona *et al.* [15] who have shown that nanocrysalline $KTaO_3$ does indeed show defect-induced ferroelectricity and magnetism below 29 K. Small doping of magnetic ions or increasing anion vacancies would then lead to the simultaneous appearance of ferroelectricity and ferromagnetism [8,15], which is the main ingredient for multiferroic behavior at relatively high temperatures in large crystals. Defect-induced ferroelectricity, or possibly multiferroicity, may find applications to develop device materials based on the active control of correlated polar defects [64].

ACKNOWLEDGMENTS

RUS facilities in Cambridge were established through support from the NERC (Grant No. NE/B505738/1) to M.A.C. E.K.H.S. thanks the Leverhulme foundation (Grant No. RPG-2012-564) and EPSRC (Grant No. EP/K009702/1) for financial support.

APPENDIX: SUPPORTING INFORMATION

A comparison of the temperature evolution of resonance frequencies near $f \sim 740$ kHz and $f \sim 820$ kHz obtained with RPS and RUS is made in Fig. 10 and in the inset, indicating that the application of an ac electric field (RPS) generates elastic resonances of the sample. However, due to the silver electrodes, frequencies are slightly shifted to lower values as shown by comparison to frequencies (black triangles in Fig. 10) obtained from the RUS spectra collected after they were removed (Fig. 11).

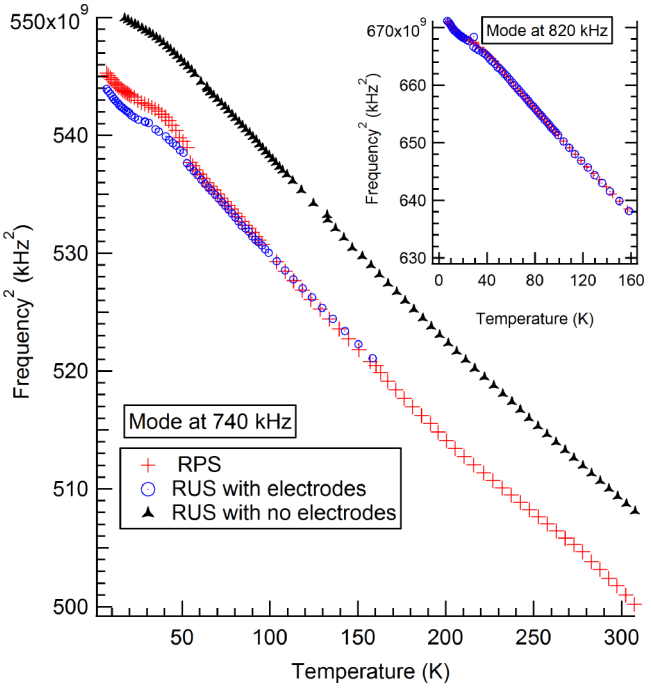

FIG. 10. (Color online) Temperature evolution of the squared frequency of an elastic resonance mode ($f \sim 740$ kHz) of single crystal $KTaO_3$ obtained using RPS (red plus signs) and RUS measurements, where the latter were performed both with (blue circles) and without (black triangles) [see Fig. 1(b) and Fig. 4]. The inset shows the temperature dependence of another resonance mode located around 820 kHz.

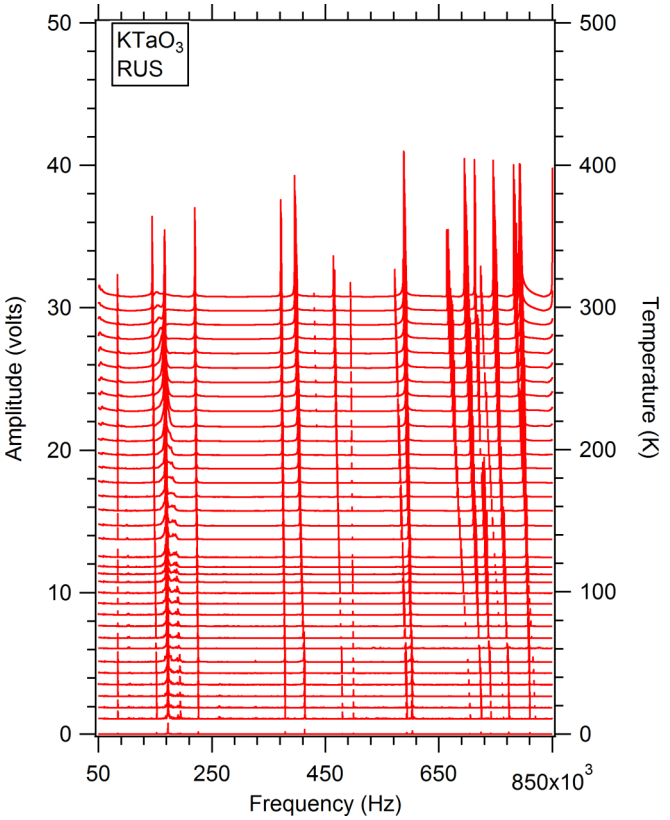

FIG. 11. (Color online) Stack of RUS spectra collected between 305 K and 8 K on a $KTaO_3$ single crystal. These measurements were performed after the removal of silver electrodes from the sample. The left vertical axis is amplitude and right vertical axis represents temperature. The spectra have been translated up the y axis in proportion to the temperature at which they were collected and the right axis has been labeled accordingly.

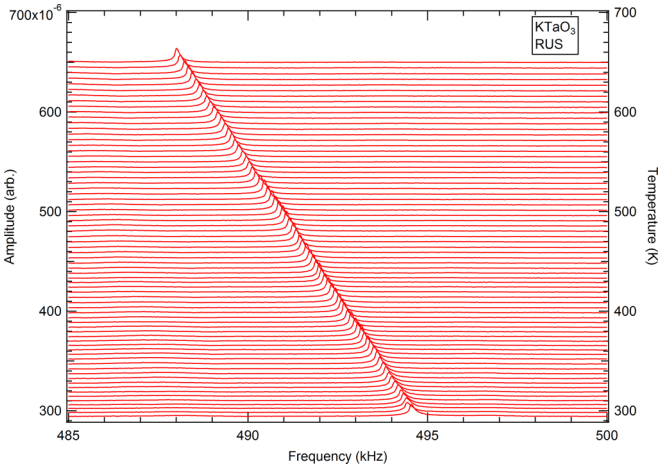

FIG. 12. (Color online) Segments of RUS spectra of $KTaO_3$ collected between 300 K and 650 K, showing the temperature evolution of a resonance mode from the sample at $\sim$ 500 kHz. Spectra shown in red correspond to heating data, whereas those in blue were collected in a cooling sequence.

In the high-temperature RUS&RPS instrument, the sample rests between the tips of two alumina rods inside the furnace with the emitter and detector transducers attached to the ends of the rods outside the furnace [46]. The RUS spectra then contain resonances both from the sample and from the rods. When a sample resonance interacts with a rod resonance, its amplitude is enhanced and the linewidth of the resulting peak does not reflect mechanical damping of the sample alone. However, it was possible to follow a resonance peak of $KTaO_3$ which did not interact in this way and its evolution with temperature between 300 and 650 K is shown in Fig. 12.

[1] S. R. Andrews, J. Phys. C: Solid State Phys. **18**, 1357 (1985).
[2] H. Uwe, K. B. Lyons, H. L. Carter, and P. A. Fleury, Phys. Rev. B **33**, 6436 (1986).
[3] J. Toulouse, P. DiAntonio, B. E. Vugmeister, X. M. Wang, and L. A. Knauss, Phys. Rev. Lett. **68**, 232 (1992).
[4] P. Voigt, K. Betzler, N. Schmidt, and S. Kapphan, Ferroelectrics **106**, 149 (1990).
[5] J. Lee, Z. Khim, Y. Park, D. Norton, N. Theodoropoulou, A. Hebard, J. Budai, L. Boatner, S. Pearton, and R. Wilson, Solid-State Electron. **47**, 2225 (2003).
[6] D. Norton, N. Theodoropoulou, A. Hebard, J. Budai, L. Boatner, S. Pearton, and R. Wilson, Electrochem. Solid State Lett. **6**, G19 (2003).
[7] I. N. Geifman and I. S. Golovina, Ferroelectrics **199**, 115 (1997).
[8] E. A. Eliseev, A. N. Morozovska, M. D. Glinchuk, and R. Blinc, J. Appl. Phys. **109**, 094105 (2011).
[9] V. V. Laguta, M. D. Glinchuk, I. P. Bykov, J. Rosa, L. Jastrabík, R. S. Klein, and G. E. Kugel, Phys. Rev. B **52**, 7102 (1995).
[10] V. V. Laguta, M. I. Zaritskii, M. D. Glinchuk, I. P. Bykov, J. Rosa, and L. Jastrabík, Phys. Rev. B **58**, 156 (1998).
[11] A. Nowick, S. Fu, W.-K. Lee, B. Lim, and T. Scherban, Mater. Sci. Eng. B **23**, 19 (1994).
[12] B. Salce, J. L. Gravil, and L. A. Boatner, J. Phys.: Condens. Matter **6**, 4077 (1994).
[13] U. Höchli, K. Knorr, and A. Loidl, Adv. Phys. **39**, 405 (1990).
[14] W. Kleemann, S. Ktz, and D. Rytz, Eur. Phys. Lett. **4**, 239 (1987).
[15] I. Golovina, S. Kolesnik, V. Bryksa, V. Strelchuk, I. Yanchuk, I. Geifman, S. Khainakov, S. Svechnikov, and A. Morozovska, Physica B **407**, 614 (2012).
[16] K. F. Wang, J. M. Liu, and Z. F. Ren, Adv. Phys. **58**, 321 (2009).
[17] M. Fiebig, J. Phys. D: Appl. Phys. **38**, R123 (2005).
[18] R. A. Cowley, S. N. Gvasaliya, S. G. Lushnikov, B. Roessli, and G. M. Rotaru, Adv. Phys. **60**, 229 (2011).
[19] B. Dkhil, P. Gemeiner, A. Al-Barakaty, L. Bellaiche, E. Dul'kin, E. Mojaev, and M. Roth, Phys. Rev. B **80**, 064103 (2009).
[20] G. A. Samara, J. Phys.: Condens. Matter **15**, R367 (2003).
[21] U. T. Hochli, H. E. Weibel, and L. A. Boatner, Phys. Rev. Lett. **39**, 1158 (1977).
[22] C. Ang, A. S. Bhalla, and L. E. Cross, Phys. Rev. B **64**, 184104 (2001).

[23] R. G. Geyer, B. Riddle, J. Krupka, and L. A. Boatner, J. Appl. Phys. **97**, 104111 (2005).
[24] S. E. Rowley, L. J. Spalek, R. P. Smith, M. P. M. Dean, M. Itoh, J. F. Scott, G. G. Lonzarich, and S. S. Saxena, Nat. Phys. **10**, 367 (2014).
[25] K. A. Müller and H. Burkard, Phys. Rev. B **19**, 3593 (1979).
[26] T. Schneider, H. Beck, and E. Stoll, Phys. Rev. B **13**, 1123 (1976).
[27] E. Salje, U. Bismayer, B. Wruck, and J. Hensler, Phase Transitions **35**, 61 (1991).
[28] S. Van Aert, S. Turner, R. Delville, D. Schryvers, G. Van Tendeloo, and E. K. H. Salje, Adv. Mater. **24**, 523 (2012).
[29] L. Goncalves-Ferreira, S. A. T. Redfern, E. Atacho, and E. K. H. Salje, Appl. Phys. Lett. **94**, 081903 (2009).
[30] E. K. H. Salje, ChemPhysChem **11**, 940 (2010).
[31] E. K. H. Salje, Annu. Rev. Mater. Res. **42**, 265 (2012).
[32] E. K. H. Salje, O. Aktas, M. A. Carpenter, V. V. Laguta, and J. F. Scott, Phys. Rev. Lett. **111**, 247603 (2013).
[33] T. Zykova-Timan and E. K. H. Salje, Appl. Phys. Lett. **104**, 082907 (2014).
[34] P. A. Fleury, J. F. Scott, and J. M. Worlock, Phys. Rev. Lett. **21**, 16 (1968).
[35] J. K. Hulm, B. T. Matthias, and E. A. Long, Phys. Rev. **79**, 885 (1950).
[36] B. E. Vugmeister and M. D. Glinchuk, Rev. Mod. Phys. **62**, 993 (1990).
[37] V. V. Laguta, M. D. Glinchuk, I. P. Bykov, J. Rosa, L. Jastrabík, M. Savinov, and Z. Trybuła, Phys. Rev. B **61**, 3897 (2000).
[38] M. D. Glinchuk, V. V. Laguta, I. P. Bykov, J. Rosa, and L. Jastrabik, J. Phys.: Condens. Matter **7**, 2605 (1995).
[39] W. Prusseit-Elffroth and F. Schwabl, Appl. Phys. A **51**, 361 (1990).
[40] O. Aktas, M. A. Carpenter, and E. K. H. Salje, Appl. Phys. Lett. **103**, 142902 (2013).
[41] O. Aktas, E. K. H. Salje, S. Crossley, G. I. Lampronti, R. W. Whatmore, N. D. Mathur, and M. A. Carpenter, Phys. Rev. B **88**, 174112 (2013).
[42] A. Migliori and J. Sarrao, *Resonant Ultrasound Spectroscopy: Applications to Physics, Materials Measurements, and Nondestructive Evaluation* (Wiley, New York, 1997).
[43] O. Aktas, E. K. H. Salje, and M. A. Carpenter, J. Phys.: Condens. Matter **25**, 465401 (2013).
[44] E. K. H. Salje, M. A. Carpenter, G. F. Nataf, G. Picht, K. Webber, J. Weerasinghe, S. Lisenkov, and L. Bellaiche, Phys. Rev. B **87**, 014106 (2013).
[45] R. E. McKnight, M. A. Carpenter, T. W. Darling, A. Buckley, and P. A. Taylor, Am. Mineral. **92**, 1665 (2007).
[46] R. E. A. McKnight, T. Moxon, A. Buckley, P. A. Taylor, T. W. Darling, and M. A. Carpenter, J. Phys.: Condens. Matter **20**, 075229 (2008).
[47] M. Fukunaga and Y. Noda, J. Phys. Soc. Jpn. **77**, 064706 (2008).
[48] S. Crossley, Ph.D. thesis, University of Cambridge, 2013).
[49] A. Nowick and B. Berry, *Anelastic Relaxation in Crystalline Solids*, Materials Science and Technology Series (Academic Press, New York, 1972).
[50] R. J. Harrison, S. A. T. Redfern, and U. Bismayer, Mineral. Mag. **68**, 839 (2004).
[51] R. I. Thomson, P. Jain, A. K. Cheetham, and M. A. Carpenter, Phys. Rev. B **86**, 214304 (2012).
[52] M. Weller, G. Y. Li, J. X. Zhang, T. S. Kê, and J. Diehl, Acta Metall. **29**, 1047 (1981).
[53] W. L. Warren, K. Vanheusden, D. Dimos, G. E. Pike, and B. A. Tuttle, J. Am. Ceram. Soc. **79**, 536 (1996).
[54] H. Abe, K. Harada, R. J. Matsuo, H. Uwe, and K. Ohshima, J. Phys.: Condens. Matter **13**, 3257 (2001).
[55] E. Salje, B. Wruck, and H. Thomas, Z. Phys. B **82**, 399 (1991).
[56] M. Born and K. Huang, *Dynamical Theory of Crystal Lattices*, International Series of Monographs on Physics (Clarendon Press, Oxford, 1954).
[57] E. Salje, *Phase Transitions in Ferroelastic and Co-elastic Crystals*, Cambridge Topics I (Cambridge University Press, Cambridge, UK, 1993).
[58] H. Yokota, Y. Uesu, C. Malibert, and J.-M. Kiat, Phys. Rev. B **75**, 184113 (2007).
[59] G. A. Samara and B. Morosin, Phys. Rev. B **8**, 1256 (1973).
[60] J. Pérez-Mato and E. K. H. Salje, Philos. Mag. Lett. **81**, 885 (2001).
[61] P. Voigt and S. Kapphan, Ferroelectrics **157**, 239 (1994).
[62] H. Yokota, H. Usami, R. Haumont, P. Hicher, J. Kaneshiro, E. K. H. Salje, and Y. Uesu, Phys. Rev. B **89**, 144109 (2014).
[63] A. K. Tagantsev and A. S. Yurkov, J. Appl. Phys. **112**, 044103 (2012).
[64] D. Lee, B. C. Jeon, S. H. Baek, S. M. Yang, Y. J. Shin, T. H. Kim, Y. S. Kim, J.-G. Yoon, C. B. Eom, and T. W. Noh, Adv. Mater. **24**, 6490 (2012).